Springer

KSME

Journal of Mechanical Science and Technology 29 (12) (2015) 5205~5215
www.springerlink.com/content/1738-494x(Print)/1976-3824(Online)
DOI 10.1007/s12206-015-0718-5

Dynamic analysis of the machine drive system †

Huiduan Zhang*

School of Mechanics and Power Engineering, Henan Polytechnic University, Jiaozuo, 454000, China

(Manuscript Received September 26, 2014; Revised March 18, 2015; Accepted April 9, 2015)

Abstract

In consideration of the bearing stiffness, the contact deformation between the ball screw and the worktable, and the contact deformation between the worktable and the guide, lateral, axial and torsional vibrations of the pre-tension screw and the vibration of the worktable were studied. A dynamic model of the ball screw drive system of machines was established by using the Lagrange equation. The model was analyzed by the mode superposition and Runge-Kutta method to calculate the transient response of the system. Effects of system's parameters on the whirl speed of the screw, the axial vibration of the cutter's work point, and also the stability of the system are discussed. The present work supplies a base for designing the drive system.

Keywords: Drive system; Whirl speed; Positioning precision; Stability

1. Introduction

The drive system of the ball screw has wide application in machine tools. With increasing of the feeding velocity and machining precision, the precision of the machine tool worktable movement and positioning become important problems, and the dynamic response of the drive system becomes more and more important.

The ball screw drive system can be seen as a rotating beam with a moving mass. Sheu and Yang [1] analyzed the whirl speed and critical speed of the spinning Rayleigh beam. Gu and Cheng [2] simplified the system of the ball screw drive as a rotating beam subjected to a moving mass and studied lateral vibration of the system. Shiaua, Huanga, Wanga and Hsub [3] investigated the dynamic response of a rotating multi-span shaft with general boundary conditions subjected to an axially moving load. Eftekhar Azama, M. Mofidb and Afghani Khoraskanic [4] analyzed the dynamic responses of a Timoshenko beam subjected to a moving mass and a moving sprung mass. The differential equations for beam vibration were derived by using Hamilton's principle and solved by using the modal superposition method. Ariaei, Ziaei-Rad and M. Ghayour [5] presented the beam equations of motion which were obtained based on the Timoshenko beam theory by including the dynamic effect of a moving mass traveling along a vibrating path.

In machine tools, the screw is often pre-tensioned to increase its lateral stiffness. Gallina [6] studied the longitudinal and torsional vibrations of the screw. Huang and Yang [7] analyzed the rotating beam subjected to repeating axial and transverse forces. The governing equations of the rotating Rayleigh beam were derived by Hamilton's principle. Stojanović´ and Kozić´[8] considered the forced vibration of a Rayleigh and Timoshenko double-beam system continuously joined by a Winkler elastic layer under compressive axial loading. They discussed vibrations of the system and formulated conditions of resonance.

When the machine runs at high speed, the stability of the system is very important. Ghayesh and Amabili [9] investigated numerically the nonlinear forced vibration and stability of an axially moving Timoshenko beam with an intra-span spring-support, which taking into account the shear deformation and rotary inertia. Tang, Chen, Zhang and Yang [10] focused on the effect of longitudinally varying tensions due to the axial acceleration and analyzed stability of axially accelerating viscoelastic Timoshenko beams. The governing equations and the accurate boundary conditions for coupled planar motion of the Timoshenko beam were established using the generalized Hamilton principle and the Kelvin viscoelastic constitutive relation. Yong, Shiau and Kuo [11] investigated the lateral vibration of a spinning disk-shaft system supported by a pair of ball bearings and subjected to a pair of random axial forces at both ends. An, Feng and Yu [12] used finite element method to analyze the ball screw feeding system's characteristic. They pointed out that increasing the diameter of the screw could improve the system's dynamic performance, but had a higher request for system stability due to inertia of

*Corresponding author. Tel.: +86 3913987411, Fax.: +86 3913987411
E-mail address: zhanghd@hpu.edu.cn
† Recommended by Associate Editor Jun-Sik Kim

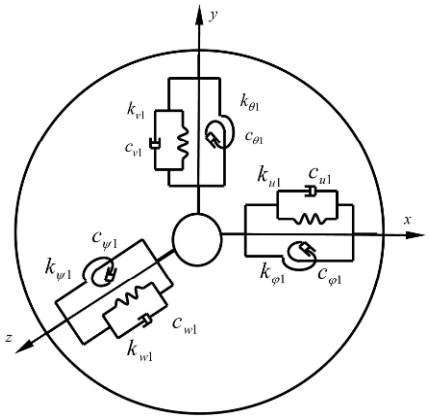

Fig. 1. The contact model of the bearing.

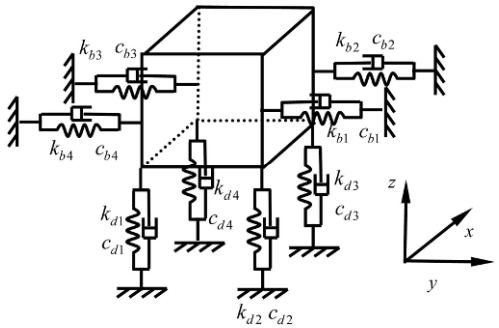

Fig. 2. The contact model between the worktable and the guide way.

the screw.

All the above works neglected contact deformation of the system, such as deformation of the worktable contacting with the guide way, and did not analyze comprehensive effect of the system vibrations on the precisions. Considering the bearing stiffness, the contact deformation between the screw and the nut, and also the contact deformation between the worktable and the guide way, the present work establishes a dynamic model of the ball screw drive system by the Lagrange equation. The model is created by mode superposition, and Runge-Kutta method is used to analyze the dynamic response of the system, including the vibration of the screw, the axial vibration amplitude of the cutter's work point, and also the stability of the drive system.

2. Dynamic model of the system

To consider the contact deformations, the bearings at both ends of the screw and the contact between the screw and the nut are expressed by six stiffness and damping coefficients respectively. Fig. 1 is the bearing's contact model, and the contact model between the screw and the nut is the same as Fig. 1, but the parameters are different. The contact model of the worktable and guide way is shown in Fig. 2. All parameters are listed in the nomenclature.

In the system, the screw rotates at a constant angular velocity Ω. The coordinate origin is at the left end of the screw. The coordinate system and the dynamic model of the system are shown in Fig. 3. The worktable translation $s(t)$ in x direction includes axial translation produced by the screw rotation, axial one $\lambda\varphi_m$ caused by torsional deformation of the screw, $u(\lambda\theta_d, t)$ from axial deformation of the screw and q_x from local vibration of the worktable, and is expressed as:

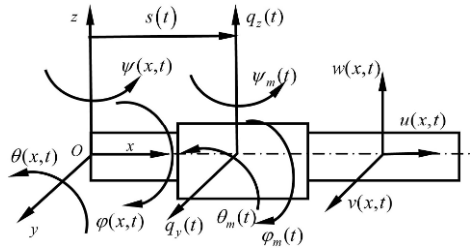

Fig. 3. The dynamic model of the drive system.

$$s(t) = \lambda\theta_d + \lambda\phi_m + u(\lambda\theta_d, t) + q_x . \tag{1}$$

Kinetic energy of the system, including the kinetic energy of the screw T_s and the kinetic energy of the worktable T_m, is expressed as:

$$T = T_s + T_m . \tag{2}$$

The system potential energy, including the screw deformation energy U_s and elastic contact energy between the system elements, such as the contact energy between the worktable and the screw U_n, the contact energy of the bearings U_b and the contact energy between the worktable and the guide way U_m, is expressed as:

$$U = U_s + U_n + U_b + U_m . \tag{3}$$

Energy dissipation of the system is caused by the contact damping between the system elements, such as the energy dissipation of the contact damping between the worktable and the screw D_n, the energy dissipation of the bearings D_b and the energy dissipation of the contact damping between the worktable and the guide way D_m, and is written as:

$$D = D_n + D_b + D_m . \tag{4}$$

Expressions of the terms of Eqs. (2)-(4) are in the Appendix. External forces of the system include the machining force exerted on the worktable and the worktable gravity, so that the virtual work of the system is:

$$\delta W = -F_m \delta s - mg\delta q_z . \tag{5}$$

From Timoshenko beam theory, displacements of lateral vibration of the screw consist of the displacement produced by the screw bending and one from the shear deformation caused by the bending, which are expressed as:

$$\begin{cases} v(x,t) = v_b(x,t) + v_s(x,t) \\ w(x,t) = w_b(x,t) + w_s(x,t) \end{cases}. \tag{6}$$

Relations of the displacements of the screw rotation around z and y axes with the bending displacements of the screw are:

$$\begin{cases} \psi(x,t) = -\dfrac{\partial v_b(x,t)}{\partial x} \\ \theta(x,t) = \dfrac{\partial w_b(x,t)}{\partial x} \end{cases}. \tag{7}$$

From the Ref. [13], the screw vibrations can be separated in time and space, which are:

$$\begin{cases} v(x,t) = V(x)q_v(t) \\ w(x,t) = V(x)q_w(t) \\ u(x,t) = U(x)q_u(t) \\ \varphi(x,t) = \Phi(x)q_\varphi(t) \\ \theta(x,t) = \Psi(x)q_\theta(t) \\ \psi(x,t) = \Psi(x)q_\psi(t). \end{cases} \tag{8}$$

First, Eqs. (1), (6)-(8) are substituted into Eqs. (2)-(4); then using Eq. (5) and the Lagrange equation yields the dynamic equation of the system:

$$[M]\{\ddot{q}\} + [C]\{\dot{q}\} + [K]\{q\} = \{F\}, \tag{9}$$

where $\{q\} = \{q_u\ q_v\ q_w\ q_\varphi\ q_\theta\ q_\psi\ s\ q_y\ q_z\ \varphi_m\ \theta_m\ \psi_m\}$, $\{\dot{q}\}$ and $\{\ddot{q}\}$ denote the velocity and acceleration, respectively. $[M]$, $[C]$ and $[K]$ express the mass, damping and stiffness matrixes of the system, and $\{F\}$ is the force vector.

3. The frequency equation and mode shape of the screw

From Ref. [5], y direction vibrations of the axially pretensioned screw are expressed as:

$$\begin{cases} \rho A\dfrac{\partial^2 v(x,t)}{\partial t^2} + GAk\left[\dfrac{\partial \psi(x,t)}{\partial x} - \dfrac{\partial^2 v(x,t)}{\partial x^2}\right] \\ -F\dfrac{\partial^2 v(x,t)}{\partial x^2} = 0 \\ \rho I\left[\dfrac{\partial^2 \psi(x,t)}{\partial t^2} - 2\mathrm{i}\Omega\dfrac{\partial \psi(x,t)}{\partial t}\right] - EI\dfrac{\partial^2 \psi(x,t)}{\partial x^2} \\ +GAk\left[\psi(x,t) - \dfrac{\partial v(x,t)}{\partial x}\right] = 0 \end{cases}. \tag{10}$$

To let solutions of Eq. (10) be: $v(x,t) = V_0 e^{px} e^{\mathrm{i}\omega t}$ and $\psi(x,t) = \Psi_0 e^{px} e^{\mathrm{i}\omega t}$. Substituting the solutions into Eq. (10) yields:

$$\begin{bmatrix} (-F - GAk)p^2 & GAkp \\ -\rho A\omega^2 & \\ GAkp & p^2 EI - GAk + \\ & \rho I\omega^2 - 2\rho I\Omega\omega \end{bmatrix} \begin{Bmatrix} V_0 \\ \Psi_0 \end{Bmatrix} = 0. \tag{11}$$

For the non-trivial solution, one has

$$\begin{vmatrix} (-F - GAk)p^2 & GAkp \\ -\rho A\omega^2 & \\ GAkp & p^2 EI - GAk + \\ & \rho I\omega^2 - 2\rho I\Omega\omega \end{vmatrix} = 0. \tag{12}$$

From Eq. (12), one can get $p = \pm\alpha$ and $p = \pm\mathrm{i}\beta$.

where $\alpha = \dfrac{-b_0 + \sqrt{b_0^2 - 4a_0c_0}}{2a_0}$,

$$\beta = \frac{b_0 + \sqrt{b_0^2 - 4a_0c_0}}{2a_0},$$

$$a_0 = (GAk + F)EI$$

$$b_0 = EI\rho A\omega^2 + (F + GAk)$$

$$(-GAk + \rho I\omega^2 - 2\rho I\Omega\omega) + (GAk)^2$$

$$c_0 = \rho A\omega^2(\rho I\omega^2 - GAk - 2\rho I\Omega\omega).$$

The mode shapes can be expressed as:

$$\begin{cases} V(x) = C_1\sin(\beta x) + C_2\cos(\beta x) + \\ \qquad C_3\sinh(\alpha x) + C_4\cosh(\alpha x) \\ \Psi(x) = \eta C_1\cos(\beta x) - \eta C_2\sin(\beta x) + \\ \qquad \delta C_3\cosh(\alpha x) + \delta C_4\sinh(\alpha x) \end{cases}. \tag{13}$$

If α is a imaginary, $\sin(\alpha)$ and $\cos(\alpha)$ replace the $\sinh(\alpha)$ and $\cosh(\alpha)$. Substituting the above expressions into Eq. (10) yields:

$$\eta = \frac{GAk\beta^2 + F\beta^2 - \rho A\omega^2}{GAk\beta} \quad \delta = \frac{GAk\alpha^2 + F\alpha^2 + \rho A\omega^2}{GAk\alpha}.$$

When the screw is supported elastically at both ends, boundary conditions of the lateral vibration are:

$$\begin{cases} EI\dfrac{\mathrm{d}\psi(0,t)}{\mathrm{d}x} = k_{\psi b}\psi(0,t) \\ kAG\left(\psi(0,t) - \dfrac{\mathrm{d}v(0,t)}{\mathrm{d}x}\right) = -k_{vb}v(0,t) - F\dfrac{\mathrm{d}v(0,t)}{\mathrm{d}x} \\ EI\dfrac{\mathrm{d}\psi(L,t)}{\mathrm{d}x} = -k_{\psi b}\psi(L,t) \\ kAG\left(\psi(L,t) - \dfrac{\mathrm{d}v(L,t)}{\mathrm{d}x}\right) = k_{vb}v(L,t) - F\dfrac{\mathrm{d}v(L,t)}{\mathrm{d}x} \end{cases}.$$

The above equations are expressed by the matrix form:

$$[A]\{c\}=0, \tag{14}$$

where $\{c\}=\{C_1\ C_2\ C_3\ C_4\}^T$. For the non-trivial solution, the coefficient matrix must be singular, so that the frequency equation is:

$$|A|=0. \tag{15}$$

Substituting Eq. (15) into Eq. (14) and setting $C_1=1$ yields the vector $\{c\}$ and the corresponding mode shapes of the lateral vibration. For the orthonormality of the mode shapes, letting $\chi_v^2\int_0^L \rho AV^2(x)dx=1$ and $\chi_\psi^2\int_0^L \rho I\Psi^2(x)dx=1$ yields:

$$\chi_v^2=\frac{1}{\int_0^L \rho AV^2(x)dx}\ ;\ \chi_\psi^2=\frac{1}{\int_0^L \rho I\Psi^2(x)dx}.$$

The orthogonal mode shapes of the lateral vibration can be expressed as:

$$\begin{cases} V(x)=\chi_v\begin{bmatrix} C_1\sin(\beta x)+C_2\cos(\beta x)+\\ C_3\sinh(\alpha x)+C_4\cosh(\alpha x)\end{bmatrix} \\ \Psi(x)=\chi_\psi\begin{bmatrix} \eta C_1\cos(\beta x)-\eta C_2\sin(\beta x)+\\ \delta C_3\cosh(\alpha x)+\delta C_4\sinh(\alpha x)\end{bmatrix}\end{cases}. \tag{16}$$

Since the axial pre-tension force does not change the dynamic models of the longitudinal and torsional vibrations of the screw, the frequency equations and mode shapes do not change. From Ref. [13], the frequency equation of the longitudinal vibration of the screw supported elastically at both ends is expressed as:

$$\left(E^2A^2\omega_u^2-k_{ub}^2a_u^2\right)\sin\frac{\omega_u}{a_u}L=2k_{ub}EA\omega_u a_u\cos\frac{\omega_u}{a_u}L. \tag{17}$$

The orthogonal mode shape is:

$$U(x)=\chi_u\left(k_{ub}a_u\sin\frac{\omega_u}{a_u}x+EA\omega_u\cos\frac{\omega_u}{a_u}x\right), \tag{18}$$

where

$$a_u=\sqrt{\frac{E}{\rho}}\ ,\ \chi_u^2=\frac{1}{\rho A\int_0^L\left(k_{ub}a_u\sin\frac{\omega_u}{a_u}x+EA\omega_u\cos\frac{\omega_u}{a_u}x\right)^2dx}.$$

The frequency equation of the torsional vibration of the screw supported elastically at both ends is:

$$\left(G^2J^2\omega_\varphi^2-k_{\varphi b}^2a_\varphi^2\right)\sin\frac{\omega_\varphi}{a_\varphi}L=2k_{\varphi b}GJ\omega_\varphi a_\varphi\cos\frac{\omega_\varphi}{a_\varphi}L. \tag{19}$$

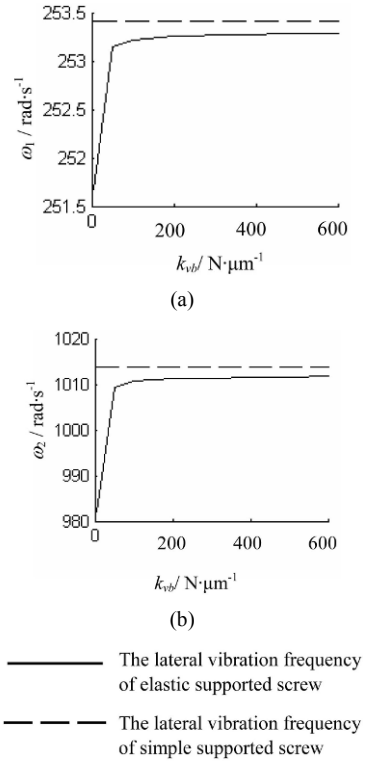

Fig. 4. The screw's lateral vibration frequency as a function of the bearing's lateral stiffness k_{vb}: (a) The first order frequency; (b) the second order frequency.

The orthogonal mode shape is:

$$\Phi(x)=\chi_\varphi\left(k_{\varphi b}a_\varphi\sin\frac{\omega_\varphi}{a_\varphi}x+GJ\omega_\varphi\cos\frac{\omega_\varphi}{a_\varphi}x\right) \tag{20}$$

where $a_\varphi=\sqrt{\frac{G}{\rho}}$;

$$\chi_\varphi^2=\frac{1}{\rho J\int_0^L\left(k_{\varphi b}a_\varphi\sin\frac{\omega_\varphi}{a_\varphi}x+GJ\omega_\varphi\cos\frac{\omega_\varphi}{a_\varphi}x\right)^2dx}.$$

4. Calculation and analysis

4.1 The whirl speed and critical speed of the screw

The forward whirl mode is primary, so the forward whirl speed and critical speed of the screw are analyzed. Letting $E=2.07\times10^5$ MPa, $G=8.3\times10^4$ Mpa, $F=0$, $\Omega=0$, $k=0.9$, $\rho=7.85\times10^3$ kg·m^{-3}, $L=1000$ mm, $d=20$ mm, $k_{\psi b}=0$, the lateral vibration frequency of the screw is calculated according to Eq. (15). The first two orders of frequency as a function of the bearing's lateral stiffness are plotted in Fig. 4. When the bearing's lateral stiffness approaches to infinity, the first two orders of frequency are closer and closer to the natural frequencies of the beam under simple supported. This means the

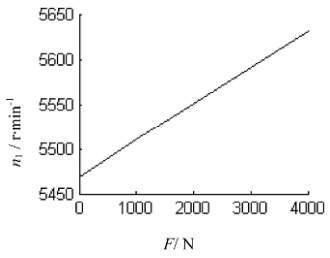

(a)

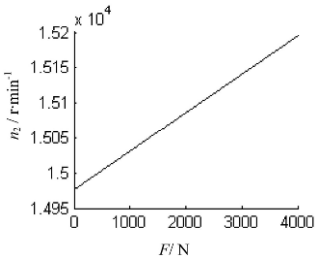

(b)

Fig. 5. The screw's whirl speed as a function of the pre-tension force F when Ω = 4000 r·min^{-1}; d = 20 mm: (a) The first order whirl speed; (b) The second order whirl speed.

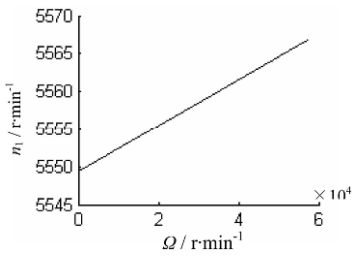

(a)

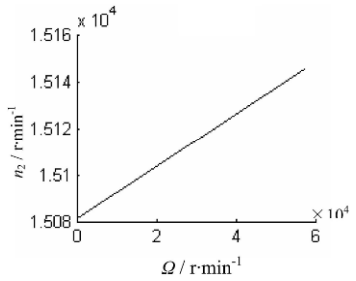

(b)

Fig. 6. The screw's whirl speed as a function of the rotational speed Ω when F = 2000 N; d= 20 mm: (a) The first order whirl speed; (b) the second order whirl speed.

work of this paper is correct.

Letting k_{vb} = 200 N·μm^{-1}, $k_{\psi b}$ = 200×10^6 N·rad^{-1}, the whirl speed of the screw is calculated as a function of the pre-tension force F, rotational speed Ω and the screw's diameter d, which are plotted in Figs. 5-7.

One can see that the whirl speed increases with an increasing of the pre-tension force F due to the lateral stiffness, of rotational speed Ω due to the gyroscopic effect, and of the screw's diameter d due to the inertia.

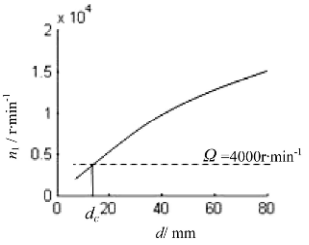

(a)

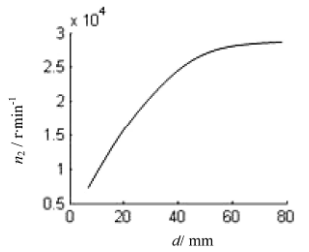

(b)

Fig. 7. The screw's whirl speed as a function of the diameter d when Ω = 4000r·min^{-1}; F = 2000 N: (a) The first order whirl speed; (b) the second order whirl speed.

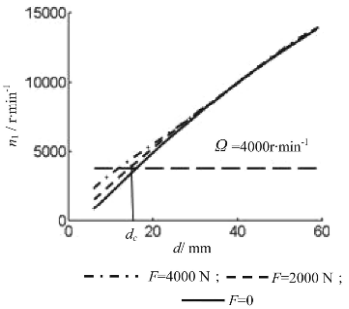

Fig. 8. The effect of pre-tension force F on the critical diameter d_c.

In Fig. 7, the screw's working rotational speed Ω = 4000 r·min^{-1}. The screw will pass though the first-order resonance in start-up when $d < d_c$ (d_c is defined as the critical diameter), and the screw will not pass though resonance in start-up when $d > d_c$, but when $d = d_c$, the screw's rotational speed is the critical speed, so the screw cannot work normally. Fig. 7 indicates that resonance can be avoided by adjusting the screw's parameters in an appropriate range.

The critical diameter of the screw's resonance varies according to different pre-tensional forces. Fig. 8 shows that the bigger the pre-tensional force is, due to increasing the lateral stiffness of the screw, the smaller d_c becomes.

Fig. 9 indicates that the whirl speed of the screw depends on the lateral supporting stiffness of the bearings. When with a low speed, the lateral supporting stiffness has little effect on d_c, but the higher the speed is, due to the gyroscopic effect, the bigger the effect is.

Fig. 10 shows that the whirl speed of the screw depends on the bearing rotational stiffness. When with a low speed, as the lateral stiffness, the bearing rotational stiffness has little effect on d_c.

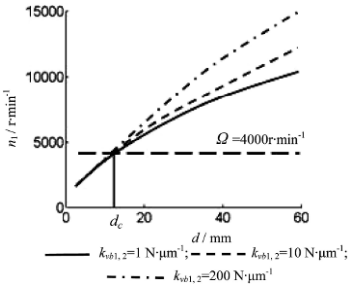

Fig. 9. The effect of the bearing's lateral stiffness on critical diameter d_c.

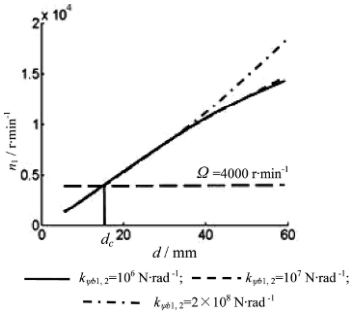

Fig. 10. The effect of the bearing's rotational stiffness on the critical diameter d_c.

Fig. 11 is the screw's whirl speed depends on the diameter d and rotational speed Ω. The screw will pass though different resonance speeds and orders if it's working rotational speed adds up to 6×10^4 r·min^{-1}. In Fig. 11(a) d = 10 mm, the screw passes through six orders resonance; but in Fig. 11(d) d = 80 mm, the screw passes through three orders resonance. When the diameter of the screw increases, the natural vibration frequency of the screw also increases. So the resonance orders decrease when it reaches the same speed.

4.2 The axial vibration amplitude of the cutter's work point

The frequencies and corresponding mode shapes are substituted into Eq. (9). Then the equation is solved by the mode superposition and Runge-Kutta method to analyze axial vibration of the cutter work point.

From Eq. (1), the worktable translation $s_1 = \lambda\theta_d$ produced by the screw rotation is linear, but the translation $s_2 = \lambda\phi_m + u(\lambda\theta_d, t) + q_x$ caused by the system vibration is fluctuant. If the distance from the cutter's work point to the joint point between the screw and the nut are R_y in y direction and the distance R_z in z direction, the worktable rotation around y and z axes can cause the work point to displace axially. Therefore, the fluctuant part of axial translation of the work point can be expressed:

$$s_v = \lambda\phi_m + u(\lambda\theta_d, t) + q_x + R_y\psi_m - R_z\theta_m . \quad (21)$$

The fluctuant part is the main factor affecting the precision of the machine tool worktable positioning. Letting $\overline{s}_v$ is the vibration amplitude of s_v, the following analysis focuses on $\overline{s}_v$.

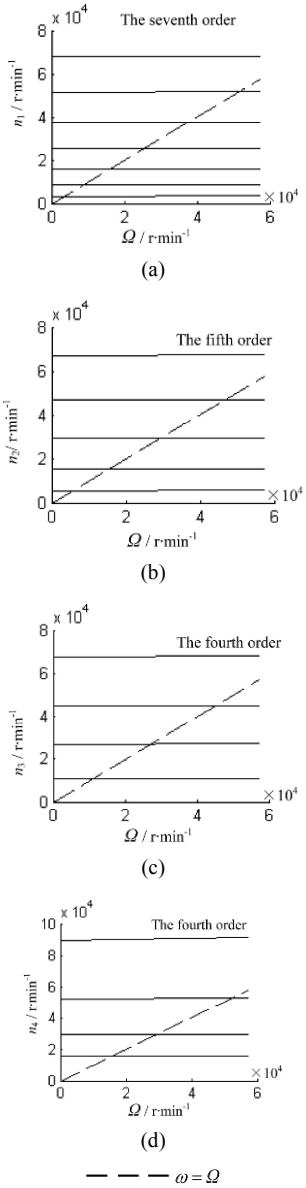

Fig. 11. The screw's whirl speed as a function of the diameter d and rotational speed Ω : (a) d = 10 mm; (b) d = 20 mm; (c) d = 40 mm; (d) d = 80 mm.

Letting Ω = 4000 r·min^{-1}, a = 300 mm, b = 200 mm, F = 2000 N, R_y = 200 mm, R_z = 200 mm, F_m = 2000 N, k_{ub} = 200 N/μm, k_{vb} = 200 N/μm, $k_{\psi b}$ = 300×10^6 N/rad, $k_{\phi b}$ = 50 N/rad, k_v = 200 N/μm, k_ψ = 300 N/μm, k_φ = 50N/rad, k_{di} = 100 N/μm, k_{bi} = 100 N/μm, i = 1, 2, 3, 4, each damping coefficient is 20 N.s/m.

The axial vibration amplitudes of the work point are predicted as shown in Figs. 12-15. Each of the figures shows that increasing the screw's diameter can contribute to decrease the axial vibration amplitude of the work point because of increasing the stiffness of the system. From Figs. 12-14, the axial vibration amplitude of the work point increases when the worktable mass increases due to the mass inertia increasing. In

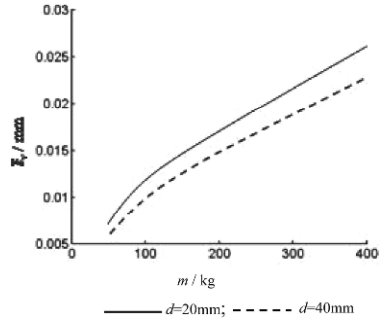

Fig. 12. The effect of worktable mass on work point axial vibration amplitude when h = 10 mm, k_u = 40 N·μm^{-1}.

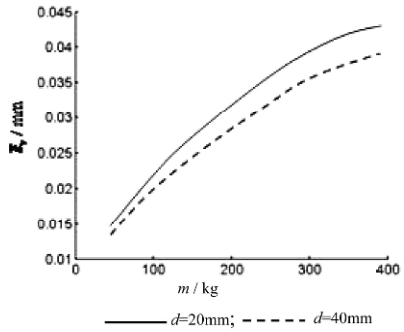

Fig. 13. The effect of worktable mass on work point axial vibration amplitude when h = 20 mm, k_u = 40 N·μm^{-1}.

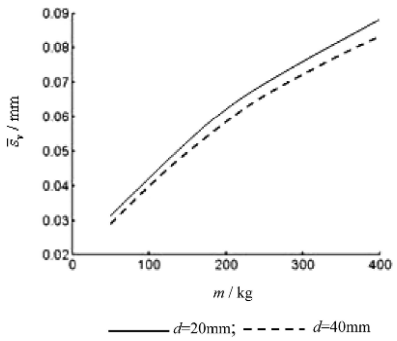

Fig. 14. The effect of worktable mass on work point axial vibration amplitude when h = 40 mm, k_u = 40 N·μm^{-1}.

Figs. 12-14, the screw lead is different, and comparing the three figures one can reach the conclusion that when the screw lead increases, the moving speed of the worktable increases, so it leads to the axial vibration amplitude of the work point increasing. Fig. 15 shows that axial contact stiffness of the screw with the nut has evident effect on the axial vibration amplitude of the work point. The large axial contact stiffness k_u of the screw with the nut can decrease the axial vibration amplitude of the work point. So the double nuts can decrease the axial fluctuate translation of the work point because of increasing the axial stiffness.

From Eq. (21), the worktable rotation around y and z axes can cause the work point to displace axially. Therefore, the larger the distances from the work point to the joint point of the worktable and the screw are, which means that R_y and

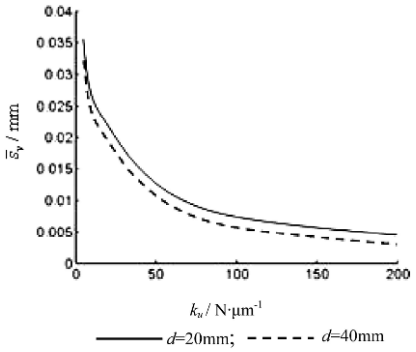

Fig. 15. The effect of axial contact stiffness between screw and nut on work point axial vibration amplitude when h = 10 mm, m = 100 kg.

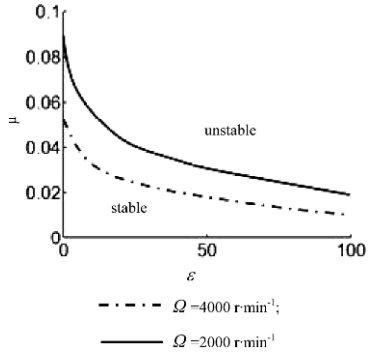

Fig. 16. The effect of the screw's rotational speed on the stable border.

R_z are larger, the larger the axial vibration of the work point is.

4.3 Analysis of the stability of the feed system

According to the Lyapunov theory, the Lyapunov function is required to analyze the stability of the system. For the non-linear system, the solution of the state transition matrix can help to judge the stability of the system. In this paper, the numerical method is used. If the working time extends infinitely, and the system is still stable, the whole system follows up; if the vibration amplitude expands infinitely following the time, the whole system is in an unstable constitution.

Through the above analysis of the screw and the worktable, the mass of the worktable and its moving speed along the screw (which is, the screw lead) have common influence on the dynamic response of the whole system. The mass ratio of the worktable to the screw is $\varepsilon = \dfrac{m}{\rho AL}$, and the ratio of the screw lead to its length is $\mu = \dfrac{h}{L}$; thus the system stability can be analyzed on the plane ε and μ during the time of $t = 3T_p$.

The effect of the screw rotational speed on the system stable border is shown in Fig. 16. The system stability weakens when the rotational speed increases for the increasing of the gyroscopic it brings. The contact stiffness of the worktable and the guide way bottom has an effect on the stable border, which is shown in Fig. 17. The effect of the axial support stiffness of the bearing is shown in Fig. 18. The effect of the

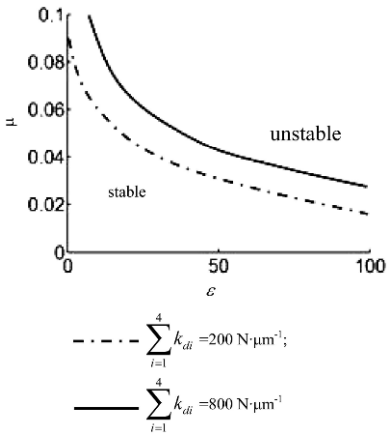

Fig. 17. The effect of the contact stiffness between the worktable and the guide bottom on the stable border.

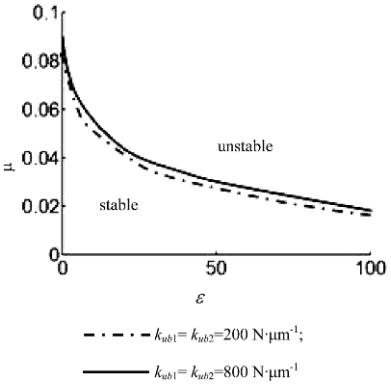

Fig. 18. The effect of the axial stiffness of the bearings on the stable border.

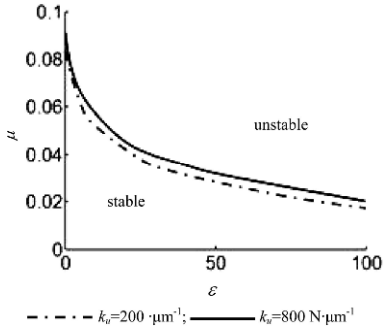

Fig. 19. The effect of the axial contact stiffness k_u between the screw and the nut on the stable border.

axial contact stiffness of the screw and the nut is shown in Fig. 19. From Figs. 17-19 one can see that increasing the contact stiffness is beneficial to the system stability, of which the contact stiffness of the worktable and the guide way bottom has its obvious effect. The effect of the screw diameter is shown in Fig. 20, and it shows that the bigger diameter of the screw also weakens the stability because of increasing the rotational inertia.

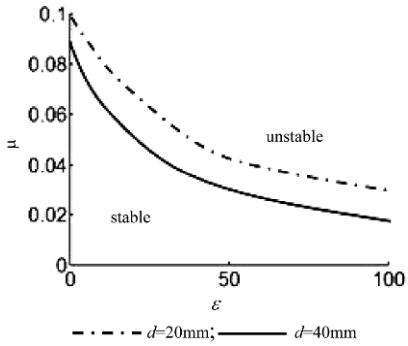

Fig. 20. The effect of the screw's diameter on the stable border.

5. Conclusions

Considering the contact deformation of the system, a dynamic model of the ball screw drive system is established by the Lagrange equation. The model is solved by the mode superposition and Runge-Kutta method. The paper discusses the whirl speed and critical speed of the screw, the axial vibration amplitude of the cutter's work point, and also analyzes the stability of the drive system. Through above analysis, the following conclusions are obtained:

The screw's whirl speed is affected by the pre-tension force, the rotational speed, the diameter of the screw and the bearing's stiffness. Resonance can be avoided by designing the system's parameters reasonably.

The axial vibration amplitude of the work point is affected by the worktable's mass, the lead of the screw, and axial contact stiffness of the screw with the nut. The positioning accuracy of the work table can be improved by increasing axial contact stiffness of the screw with the nut and the screw's diameter or decreasing screw's lead.

To increase the system stability, one can increase the contact stiffness of the system, especially the contact stiffness of the worktable and the guide way bottom, and also can decrease the rotational speed or the diameter of the screw.

Acknowledgment

This work supported by Henan Polytechnic University under Contract No.B2011-92, China.

Nomenclature

t : Time

s , q_y , q_z : Displacements of the worktable in x, y, and z directions, respectively

φ_m , θ_m , ψ_m : Angular displacements of the worktable around x, y and z axes, respectively

$u(x,t)$: Axial displacement of the screw in x direction

$v(x,t)$, $w(x,t)$: Lateral displacements of the screw in y and z directions, respectively

$\varphi(x,t)$: Torsional angle of the screw around x axis

$\theta(x,t)$, $\psi(x,t)$: Rotational angles of the screw around y and z

axes, respectively

s_v, $\overline{s}_v$: Fluctuant displacement and it's amplitude of the cutter work point in x direction, respectively

k_{ub} : Axial stiffness coefficient of the screw bearings in x direction

k_{vb} : Lateral stiffness coefficient of the screw bearings in y and z directions

$k_{\varphi b}$: Torsional stiffness coefficient of the screw bearings around x axis

$k_{\psi b}$: Rotational stiffness coefficient of the bearings around y and z axes

c_{ub} : Axial damping coefficient of the bearings in x direction

c_{vb} : Lateral damping coefficient of the bearings in y and z directions

$c_{\varphi b}$: Torsional damping coefficient of the bearings around x axis

$c_{\psi b}$: Rotational damping coefficient of the bearings around y and z axes

k_u : Contact stiffness coefficient between the screw and nut in x direction

k_v : Contact stiffness coefficient between the screw and nut in y and z directions

k_φ : Contact stiffness coefficient between the screw and nut around x axis

k_ψ : Contact stiffness coefficient between the screw and nut around y and z axes

c_u : Contact damping coefficient between the screw and nut in x direction

c_v : Contact damping coefficient between the screw and nut in y and z directions

c_φ : Contact damping coefficient between the screw and nut around x axis

c_ψ : Contact damping coefficient between the screw and nut around y and z axes

k_{d1}, k_{d2}, k_{d3}, k_{d4} : Contact stiffness coefficients between the worktable bottom and the guide way

k_{b1}, k_{b2}, k_{b3}, k_{b4} : Contact stiffness coefficients between the worktable sides and the guide way

c_{d1}, c_{d2}, c_{d3}, c_{d4} : Contact damping coefficients between the worktable bottom and the guide way

c_{b1}, c_{b2}, c_{b3}, c_{b4} : Contact damping coefficients between the worktable sides and the guide way

m : Worktable mass

h : Lead of the screw

L : Screw length

E : Young's modulus of the screw material

G : Shear modulus of the screw material

ρ : Density of the screw material;

k : Cross-section shape factor of the screw

d : Diameter of the screw

A : Cross section area of the screw, $A = \dfrac{\pi d^2}{4}$

I : Second moment of inertia of the screw, $I = \dfrac{\pi d^4}{64}$

J : Polar moment of inertia of the screw, $J = \dfrac{\pi d^4}{32}$

Ω : Rotational speed of the screw

θ_d : Rotational angle of the screw, $\theta_d = \Omega t$

ω : Lateral vibration frequency of the screw

ω_u : The axial vibration frequency of the screw

ω_φ : Torsional vibration frequency of the screw

n : Whirl speed of the screw

λ : Speed coefficient of the worktable moving along the screw, $\lambda = \dfrac{h}{2\pi}$

T_p : Period of the worktable moving along the screw, $T_p = \dfrac{2\pi L}{h\Omega}$

a: Length of the worktable in x direction

b : Length of the worktable in y direction

I_x, I_y, I_z : Moments of inertia of the worktable around x, y, z axes, respectively,

$$I_x = \frac{m}{12}\left(\frac{b}{2}\right)^2,\ I_y = \frac{m}{12}\left(\frac{a}{2}\right)^2,\ I_z = \frac{m}{12}\left[\left(\frac{a}{2}\right)^2 + \left(\frac{b}{2}\right)^2\right]$$

R_y : Distance between the cutter work point and the joint point of the screw with the nut in y direction

R_z : Distance between the cutter work point and the joint point of the screw with the nut in z direction

F_m : Load exerted on the worktable

F : Axial pre-tension force of the screw

μ : Ratio of the screw's lead to its length

ε : Ratio of the worktable's mass to the screw's mass

References

[1] G. J. Sheu and S. M. Yang, Dynamic analysis of a spinning Rayleigh beam, *International J. of Mechanical Sciences,* 47 (2005) 157-169.

[2] U. C. Gu and C. C. Cheng, Vibration analysis of a high-speed spindle under the action of a moving mass, *J. Journal of Sound and Vibration,* 278 (2004) 1131-1146.

[3] T. N. Shiaua, K. H. Huanga, F. C. Wanga and W. C. Hsub, Dynamic response of a rotating multi-span shaft with general boundary conditions subjected to a moving load, *J. of Sound and Vibration,* 323 (2009) 1045-1060.

[4] S. E. Azama, M. Mofidb and R. A. Khoraskanic, Dynamic response of Timoshenko beam under moving mass, *J. Scientia Iranica,* 20 (1) (2013) 50-56.

[5] A. Ariaei, S. Ziaei-Rad and M. Ghayour, Repair of a cracked Timoshenko beam subjected to a moving mass using piezoelectric patches, *International J. of Mechanical Sciences,* 52 (2010) 1074-1091.

[6] P. Gallina, Vibration in screw jack mechanisms: experimental results, *J. of Sound and Vibration,* 282 (2005) 1025-1041.

[7] Y. M. Huang and M. L. Yang, Dynamic analysis of a rotating beam subjected to repeating axial and transverse forces for simulating a lathing process, *International J. of Mechanical Sciences,* 51 (2009) 256-268.

[8] V. Stojanović and P. Kozić, Forced transverse vibration of Rayleigh and Timoshenko double-beam system with effect of compressive axial load, *International J. of Mechanical Sciences,* 60 (2012) 59-71.

[9] M. H. Ghayesh and M. Amabili, Nonlinear vibrations and stability of an axially moving Timoshenko beam with an intermediate spring support, *J. Mechanism and Machine Theory,* 67 (2013) 1-16.

[10] Y. Q. Tang, L. Q. Chen, H. J. Zhang and S. P. Yang, Stability of axially accelerating viscoelastic Timoshenko beams: Recognition of longitudinally varying tensions, *J. Mechanism and Machine Theory,* 62 (2013) 31-50.

[11] T. H. Yong, T. N. Shiau and Z. H. Kuo, Dynamic stability of rotor-bearing systems subjected to random axial forces, *J. Journal of Sound and Vibration,* 305 (2007) 467-480.

[12] Q. An, P. Feng and D. Yu, Analysis of dynamic characteristic of ball screw feeding system based on FEM, *J. Manufacturing Technology and Machine Tool,* 10 (2006) 85-89 (in Chinese).

[13] Y. Zhang, *Mechanics of Mechanical Vibration*, Jilin Science &Technology Press, Changchun (2000) (in Chinese).

Appendix

The energy expressions in Eqs. (2)-(4)

$$T_s=\frac{1}{2}\int_0^L\rho A\left[\left(\frac{\partial v(x,t)}{\partial t}\right)^2+\left(\frac{\partial w(x,t)}{\partial t}\right)^2\right]\mathrm{d}x+\frac{1}{2}\int_0^L\rho I\left[\left(\frac{\partial\theta(x,t)}{\partial t}\right)^2+\left(\frac{\partial\psi(x,t)}{\partial t}\right)^2\right]\mathrm{d}x+\frac{1}{2}\int_0^L\rho J\dot{\theta}_d\left[\left(-\frac{\partial\theta(x,t)}{\partial t}\right)\psi(x,t)+\left(\frac{\partial\psi(x,t)}{\partial t}\right)\theta(x,t)\right]\mathrm{d}x+\frac{1}{2}\int_0^L\rho J\left[\dot{\theta}_d+\frac{\partial\varphi(x,t)}{\partial t}\right]^2\mathrm{d}x+\frac{1}{2}\int_0^L\rho A\left[\frac{\partial u(x,t)}{\partial t}\right]^2\mathrm{d}x$$

$$T_m=\frac{1}{2}m\left[\dot{s}^2+\left(\dot{q}_y\right)^2+\left(\dot{q}_z\right)^2\right]+\frac{1}{2}I_x\left(\dot{\varphi}_m\right)^2+\frac{1}{2}I_y\left(\dot{\theta}_m\right)^2+\frac{1}{2}I_z\left(\dot{\psi}_m\right)^2$$

$$U_s=\frac{1}{2}\int_0^L EI\left[\left(\frac{\partial\theta(x,t)}{\partial x}\right)^2+\left(\frac{\partial\psi(x,t)}{\partial x}\right)^2\right]\mathrm{d}x+\frac{1}{2}\int_0^L kAG\left[\left(\frac{\partial v_s(x,t)}{\partial x}\right)^2+\left(\frac{\partial w_s(x,t)}{\partial x}\right)^2\right]\mathrm{d}x+\frac{1}{2}\int_0^L EA\left[\frac{\partial u(x,t)}{\partial x}\right]^2\mathrm{d}x+\frac{1}{2}\int_0^L GJ\left[\frac{\partial\varphi(x,t)}{\partial x}\right]^2\mathrm{d}x+\frac{1}{2}F\int_0^L\left[\left(\frac{\partial v(x,t)}{\partial x}\right)^2+\left(\frac{\partial w(x,t)}{\partial x}\right)^2\right]\mathrm{d}x$$

$$U_n=\frac{1}{2}k_u\left[s-\lambda\theta_d-\lambda\varphi_m-u(\lambda\theta_d,t)\right]^2+\frac{1}{2}k_v\left(q_y-v(\lambda\theta_d,t)\right)^2+\frac{1}{2}k_w\left(q_z-w(\lambda\theta_d,t)\right)^2+\frac{1}{2}k_\varphi\left[\varphi_m-\varphi(\lambda\theta_d,t)\right]^2+\frac{1}{2}k_\theta\left[\theta_m-\theta(\lambda\theta_d,t)\right]^2+\frac{1}{2}k_\psi\left[\psi_m-\psi(\lambda\theta_d,t)\right]^2$$

$$U_b=\frac{1}{2}k_{v1}\left[v(0,t)\right]^2+\frac{1}{2}k_{v2}\left[v(L,t)\right]^2+\frac{1}{2}k_{w1}\left[w(0,t)\right]^2+\frac{1}{2}k_{w2}\left[w(L,t)\right]^2+\frac{1}{2}k_{u1}\left[u(0,t)\right]^2+\frac{1}{2}k_{u2}\left[u(L,t)\right]^2+\frac{1}{2}k_{\varphi1}\left[\varphi(0,t)\right]^2+\frac{1}{2}k_{\varphi2}\left[\varphi(L,t)\right]^2+\frac{1}{2}k_{\theta1}\left[\theta(0,t)\right]^2+\frac{1}{2}k_{\theta2}\left[\theta(L,t)\right]^2+\frac{1}{2}k_{\psi1}\left[\psi(0,t)\right]^2+\frac{1}{2}k_{\psi2}\left[\psi(L,t)\right]^2$$

$$U_m=\frac{1}{2}\sum_{i=1}^4k_{di}q_z^2+\frac{1}{2}\sum_{i=1}^4k_{bi}q_y^2+\frac{1}{2}\left(k_{d1}+k_{d4}\right)\left(\frac{b}{2}\varphi_m\right)^2+\frac{1}{2}\left(k_{d2}+k_{d3}\right)\left(-\frac{b}{2}\varphi_m\right)^2+\frac{1}{2}\left(k_{d3}+k_{d4}\right)\left(\frac{a}{2}\theta_m\right)^2+\frac{1}{2}\left(k_{d1}+k_{d2}\right)\left(-\frac{a}{2}\theta_m\right)^2+\frac{1}{2}\left(k_{b2}+k_{b4}\right)\left(\frac{a}{2}\psi_m\right)^2+\frac{1}{2}\left(k_{b1}+k_{b3}\right)\left(-\frac{a}{2}\psi_m\right)^2$$

$$D_n=\frac{1}{2}c_u\left[\dot{s}-\lambda\dot{\theta}_d-\lambda\dot{\phi}_m-\frac{\mathrm{d}u(\lambda\theta_d,t)}{\mathrm{d}t}\right]^2+\frac{1}{2}c_v\left(\dot{q}_y-\frac{\mathrm{d}v(\lambda\theta_d,t)}{\mathrm{d}t}\right)^2+\frac{1}{2}c_w\left(\dot{q}_z-\frac{\mathrm{d}w(\lambda\theta_d,t)}{\mathrm{d}t}\right)^2+\frac{1}{2}c_\varphi\left[\dot{\varphi}_m-\frac{\mathrm{d}\varphi(\lambda\theta_d,t)}{\mathrm{d}t}\right]^2+\frac{1}{2}c_\theta\left[\dot{\theta}_m-\frac{\mathrm{d}\theta(\lambda\theta_d,t)}{\mathrm{d}t}\right]^2+\frac{1}{2}c_\psi\left[\dot{\psi}_m-\frac{\mathrm{d}\psi(\lambda\theta_d,t)}{\mathrm{d}t}\right]^2$$

$$D_b=\frac{1}{2}c_{u1}\left[\frac{\mathrm{d}u(0,t)}{\mathrm{d}t}\right]^2+\frac{1}{2}c_{u2}\left[\frac{\mathrm{d}u(L,t)}{\mathrm{d}t}\right]^2+\frac{1}{2}c_{v1}\left[\frac{\mathrm{d}v(0,t)}{\mathrm{d}t}\right]^2+\frac{1}{2}c_{v2}\left[\frac{\mathrm{d}v(L,t)}{dt}\right]^2+\frac{1}{2}c_{w1}\left[\frac{\mathrm{d}w(0,t)}{\mathrm{d}t}\right]^2+\frac{1}{2}c_{w2}\left[\frac{\mathrm{d}w(L,t)}{\mathrm{d}t}\right]^2+\frac{1}{2}c_{\varphi1}\left[\Omega+\frac{\mathrm{d}\varphi(0,t)}{\mathrm{d}t}\right]^2+\frac{1}{2}c_{\varphi2}\left[\Omega+\frac{\mathrm{d}\varphi(L,t)}{\mathrm{d}t}\right]^2+\frac{1}{2}c_{\theta1}\left[\frac{\mathrm{d}\theta(0,t)}{\mathrm{d}t}\right]^2+\frac{1}{2}c_{\theta2}\left[\frac{\mathrm{d}\theta(L,t)}{\mathrm{d}t}\right]^2+\frac{1}{2}c_{\psi1}\left[\frac{\mathrm{d}\psi(0,t)}{\mathrm{d}t}\right]^2+\frac{1}{2}c_{\psi2}\left[\frac{\mathrm{d}\psi(L,t)}{\mathrm{d}t}\right]^2$$

$$D_m = \frac{1}{2}\sum_{i=1}^{4} c_{di}\dot{q}_z^2 + \frac{1}{2}\sum_{i=1}^{4} c_{bi}\dot{q}_y^2 + \frac{1}{2}(c_{d1}+c_{d4})\left(\frac{b}{2}\dot{\varphi}_m\right)^2 + \frac{1}{2}(c_{d2}+c_{d3})\left(-\frac{b}{2}\dot{\varphi}_m\right)^2 + \frac{1}{2}(c_{d3}+c_{d4})\left(\frac{a}{2}\dot{\theta}_m\right)^2 + \frac{1}{2}(c_{d1}+c_{d2})\left(-\frac{a}{2}\dot{\theta}_m\right)^2 + \frac{1}{2}(c_{b2}+c_{b4})\left(\frac{a}{2}\dot{\psi}_m\right)^2 + \frac{1}{2}(c_{b1}+c_{b3})\left(-\frac{a}{2}\dot{\psi}_m\right)^2$$

Huiduan Zhang has a Doctor of Engineering in Machine Design and Theory, and is vice professor of the School of Mechanical and Power Engineering in Henan Polytechnic University. Her research interests include mechanical design, dynamics of mechanical drive system, and simulation of the mechanical system.